0023-6837/02/8208-999$03.00/0
LABORATORY INVESTIGATION
Vol. 82, No. 8, p. 999, 2002
Printed in U.S.A.

Renal Injury in Apolipoprotein E–Deficient Mice

Min Wen, Stephan Segerer, Marcio Dantas, Paul A. Brown, Kelly L. Hudkins, Tracy Goodpaster, Elizabeth Kirk, Renée C. LeBoeuf, and Charles E. Alpers

Department of Pathology (MW, SS, MD, KLH, TG, CEA) and Department of Medicine (EK, RCL), University of Washington, Seattle, Washington; and Department of Pathology (PAB), University of Aberdeen, Aberdeen, United Kingdom

SUMMARY: Hyperlipidemia is thought to accelerate the progression of renal diseases, but the mechanisms by which hyperlipidemia exerts its deleterious effect is still poorly understood. The aim of this study was to describe the renal pathology in a hyperlipidemic mouse strain, the apolipoprotein E–deficient mice (apoE-/-). Renal specimens from a total of 34 mice were studied, including 19 apoE-/- females at the age of 36 weeks, 9 apoE-/- females at the age of 24 weeks, and 6 wild-type females (C57BL/6) as controls. Kidneys were evaluated by histologic examination, immunohistochemistry, and electron microscopy. Immunohistochemistry was used to detect MAC-2–expressing monocyte/macrophages, and the proliferation marker PCNA. Glomerular cell number, glomerular matrix area, and glomerular area were quantified by morphometry. Glomerular lesions in apoE-/- mice were characterized by macrophage accumulation, commonly with foam cell appearance, deposition of extracellular matrix, glomerular hyperplasia, and at times prominent mesangiolysis associated with capillary microaneurysms. Some cases demonstrated lipid deposits filling glomerular capillaries. Arterioles of the vascular pole demonstrated a "foamy" degeneration of smooth muscle cells. These lesions related to hyperlipidemia in this well-established mouse strain have not been previously described. Because this mouse strain is among the most widely studied for interventions aimed at altering hyperlipidemia and the progression of atherosclerosis, we believe that our observations may be of major importance for the accurate interpretation of interventional studies in this strain and offer a new opportunity to study mechanisms of hyperlipidemic renal injury. (*Lab Invest 2002, 82:999–1006*).

An increasing number of studies indicate a role of hyper/dyslipidemia as a risk factor for the progression of renal diseases (Attman et al, 1999; Keane, 2000; Stevenson and Kaysen, 1999). One example is diabetic nephropathy, in which hyperlipidemia has been demonstrated to be associated with albuminuria, and in which pharmacologic reduction of lipid levels decreases urinary protein excretion (reviewed in Stevenson and Kaysen, 1999). Although the role of dyslipidemia as a cardiovascular risk factor in the general population is well established, the consequences for the development and progression of renal diseases are still poorly understood (Majumdar and Wheeler, 2000).

ApoE-/- mice have become a standard model for studies of atherosclerosis (Fazio and Linton, 2001). ApoE mediates the clearance of remnant lipoproteins via the liver (Mahley and Huang, 1999). Consequently, apoE-/- mice develop severe hyperlipidemia due to an accumulation of chylomicrons and VLDL remnant lipoproteins resembling human type III hyperlipidemia (Ghiselli et al, 1981; Plump et al, 1992). Atherosclerotic lesions at the aortic root and widespread complex plaques develop in these mice under normal chow diet, and this process is accelerated by a high fat diet (Nakashima et al, 1994; Reddick et al, 1994). Although this mouse strain is widely used for studies of atherogenesis and, recently, for studies of the combined effects of hyperlipidemia and hypertension on the kidney, no detailed description is currently available of the renal pathology in apoE-/- mice (Knowles et al, 2000). A study recently described renal injury in mice deficient in both apoE and endothelial nitric oxide synthase (Knowles et al, 2000). The authors found a decreased kidney weight, increased plasma creatinine, and an increased number of glomeruli with lipid deposits in double knockout mice at the age of 4 months (Knowles et al, 2000). A small number of glomeruli with lipid deposits were described in control apoE-/- mice, but the pathology in these mice was not fully addressed (Knowles et al, 2000).

Here we describe the renal pathology of apoE-/- mice at two time points. We identified a striking pattern of glomerular injury characterized by glomerular macrophage infiltration with accumulation of foam cells, foci of mesangiolysis, focal intracapillary lipid deposits that resemble the human lesion of lipoprotein glomerulopathy, and foam cell transformation of arteriolar smooth muscle cells in glomerular hilar arterioles. These findings provide a basis for the use of the apoE-/- mouse as a model to define mechanisms of hyperlipidemic renal injury.

DOI: 10.1097/01.LAB.0000022222.03120.D4

Received January 16, 2002.
This work was supported by NIH grants HL52848 and DK 47659. SS was supported by a grant from the Else Kröner-Fresenius-Stiftung, Bad Homburg v. d. Höhe, Germany. PAB was supported by a Peel Traveling Fellowship.
Address reprint requests to: Dr. Charles E. Alpers, University of Washington Medical Center, Department of Pathology, Box 356100, 1959 NE Pacific Street, Seattle, WA 98195. E-mail: calp@u.washington.edu

Results

ApoE-/- Mice Develop Progressive Glomerular and Arteriolar Lesions

The renal morphology and correlative studies of plasma were evaluated at the age of 24 and 36 weeks. At both time points apoE-/- mice showed a strong increase of total cholesterol as compared with wild-type controls, but measurements of glucose triglycerides did not vary significantly among the study groups (Table 1). A striking morphologic alteration was the presence of glomerular foam cells in mesangial areas, within glomerular capillary lumina, and within the glomerular stalk close to the vascular pole (Fig. 1, A and B). These foam cells contributed to the appearance of an expanded mesangium, but because of variable degrees of mesangiolysis and resultant distortion of architectural boundaries of the mesangium that were present in some animals, the distinct localization of foam cells either to mesangial areas or to adjacent capillary lumina could not always be accomplished. Figure 2B illustrates that in some cases a large proportion of the glomerular foam cells could be localized to the mesangium, where they contribute to the expansion process. Glomerular foam cells were detected in all apoE-/- mice at both time points, whereas foam cells were not detected in wild-type controls. The percentage of glomeruli with foam cells rose significantly from 7% at 24 weeks to 29% at 36 weeks of age (Figs. 2 and 3; Table 2). A clear colocalization was demonstrated between foam cells and immunohistochemically labeled monocyte/macrophages on serial tissue sections (Fig. 3), establishing the identity of foam cells as lipid-laden monocyte/macrophages. Glomerular infiltration with monocyte/macrophages was a prominent feature in apoE-/- mice. The mean number of monocyte/macrophages rose from 2.5 at 24 weeks of age to 4.3 cells per glomerulus at 36 weeks (Table 2).

In addition to foam cells within glomeruli, lipid deposits and foam cells were present in the arteriolar walls in the vascular pole (Fig. 1B). These lesions were present in 26% of the glomeruli at the age of 24 weeks, and the number of involved glomeruli rose to 59% at the age of 36 weeks (Table 2). ApoE-/- mice demonstrated widening of the mesangium due to an increase of argyrophilic matrix, as revealed by histologic stains with silver methenamine (Fig. 1C). Involved glomeruli demonstrated at times a prominent ballooning of the capillaries, which was associated with features of adjacent mesangiolysis (Fig. 1D). Mesangiolysis, defined as loss or dissolution of the normally compact silver staining mesangial matrix, was present in 7 of 18 specimens at the age of 36 weeks, whereas mesangiolysis was not detected in apoE-/- mice at 24 weeks nor in wild-type controls. Lipid droplets filling glomerular capillary lumina were detected only in apoE-/- mice at the age of 36 weeks, a finding that was present in 9 of 18 cases (Fig. 1E). These thrombus-like structures commonly showed a laminated appearance (Fig. 1E). Global glomerulosclerosis was not detected. The tubulointerstitium was well preserved in all cases without prominent interstitial leukocytic infiltrates or interstitial fibrosis.

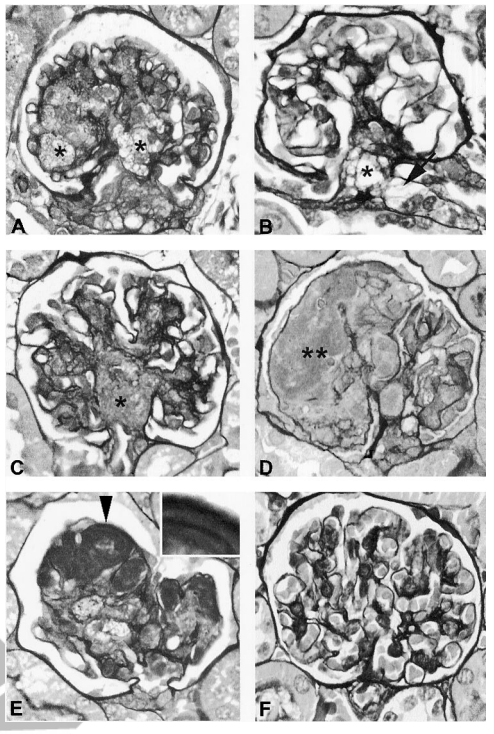

Figure 1.

Typical renal lesions in apoE-/-. Renal specimens from apoE-/- mice at the age of 36 weeks (A, C, D, and E), from an apoE-/- mouse at the age of 24 weeks (B), and a wild-type control at the age of 36 weeks (F; all original magnification, ×600, silver). A, Several foam cells are present in the glomerular tuft (*stars*). B, Lipid deposits are present in the juxtaglomerular area (*star*). The adjacent arteriolar wall demonstrates a foam cell appearance (*arrow*). C, There is prominent widening of the mesangial area (compare with the wild-type in F). D, Mesangiolysis (*double star*) and ballooning dilatation ("microaneurysm" formation) of adjacent glomerular capillaries is present. E, Capillaries are occluded by thrombus-like structures. The "thrombi" illustrated in E show multiple layers at higher magnification (*arrowhead* and insert) with adjacent foam cells in the mesangium.

Table 1. Clinical Data of the Study Groups

	C57BL/6	apoE−/−	apoE−/−
Age (weeks)	36	24	36
n =	6	10	18
Glucose (mg/dl)[a]	158.7 (± 6.8)	144.5 (± 26)	167.4 (± 24.1)
Total cholesterol (mg/dl)[a]	67 (± 8.1)	337 (± 51.2)	322 (± 51.1)
Triglycerides (mg/dl)[a]	57 (± 23.7)	48.6 (± 18.4)	46 (± 14.4)

[a] ± standard deviation.

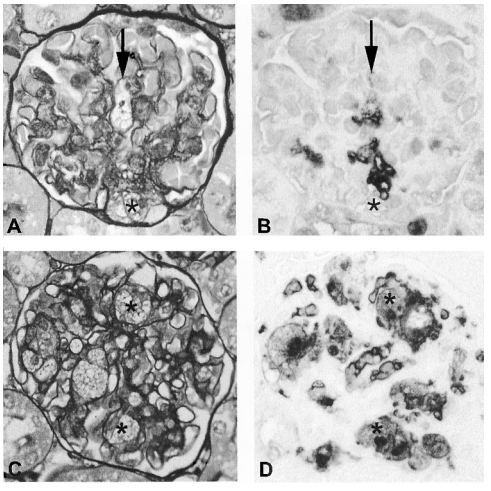

Figure 2.
Colocalization of foam cells and monocyte/macrophages. Serial sections of renal specimens from apoE-/- mice at the age of 24 weeks (A and B) and 36 weeks (C and D) stained with silver (A and C) and by immunohistochemistry for monocyte/macrophages (B and D; all original magnification, ×600). Note that cells with foam cell appearance in A and C (*stars* and *arrow*) express the monocyte/macrophage marker MAC-2 in B and D.

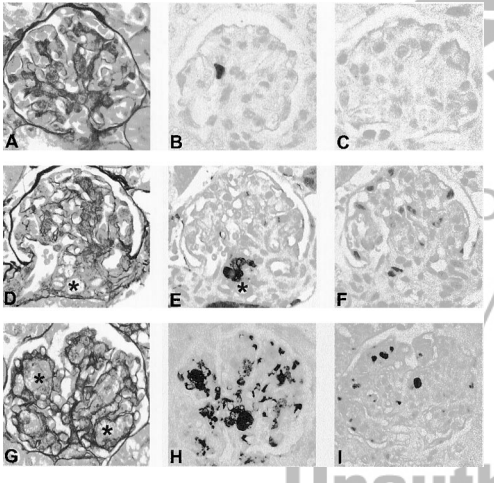

Figure 3.
Time course of the glomerular lesions in apoE-/- mice. Renal specimens from a C57BL/6 wild-type control (A, B, and C), apoE-/- mice at the age of 24 weeks (D, E, and F) and 36 weeks (G, H, and I; all original magnification, ×600). Slides were stained with silver (A, D, and G) and by immunohistochemistry for monocyte/macrophages (B, E, and H) and the proliferation marker PCNA (C, F, and I). At 36 weeks, a large number of foam cells can be detected (G, *stars*), which stain positive for MAC-2 (H) on serial sections. No glomerular foam cells are present in the control (A). Lipid deposits and foam cells are present (D and E, *stars*). Several proliferating cells can be detected at 36 weeks (I) but not in the wild-type control (C).

Glomerular Cellularity and Extracellular Matrix Are Increased in apoE-/- Mice

Glomerular tuft area, cellularity, and matrix deposition were quantified by morphometry. The morphometric analysis demonstrated an increase of the glomerular tuft area, which progressed significantly from 24 weeks of age to 36 weeks in apoE-/- mice (Table 2).

The increase of the mean cell numbers per glomerulus (Fig. 4A) was more prominent than the increase of cells per tuft area (Fig. 4B), reflecting the increased size of the glomerular tuft. Both the absolute and the relative glomerular cell number were significantly higher in apoE-/- mice compared with wild-type controls. This was consistent with an increased number of glomerular cells expressing the cell proliferation marker PCNA (Fig. 3). In addition to the increased cellularity, glomeruli from apoE-/- mice demonstrated a significantly increased glomerular matrix (Fig. 4, C and D). Both the absolute matrix area per glomerulus, and the percentage of matrix per glomerular tuft, were significantly increased. The increase in glomerular matrix was already present at 24 weeks of age compared with wild-type controls.

Characterization of several components of the increased matrix is demonstrated in Figure 5. ApoE-/- mice at 24 and 36 weeks demonstrate progressively increased mesangial accumulation of laminin and collagen IV, as revealed by immunohistochemical labeling.

Ultrastructural Features of apoE-/- Mice

Selected cases were further studied by transmission electron microscopy. Consistent with the light microscopic findings, lipid-laden cells with multiple vacuoles were present in the juxtaglomerular areas (Fig. 6A) and in the mesangium of glomerular tufts (Fig. 6B). Extracellular lipid within the mesangium was focally present (Fig. 6A). These cells were not detected in wild-type controls (Fig. 6C). Vacuoles indicative of lipid were present in smooth muscle cells of arteriolar walls. Extracellular lipid deposits and foam cells also were present in the juxtaglomerular area, adjacent to the vascular pole (Fig. 6A). At 36 weeks of age, lipid deposits were detectable in the extracellular mesangial matrix surrounding mesangial cells, in addition to lipid within foam cells. Intracapillary thrombus-like structures, detailed by histologic examination, were shown at times to have a laminated appearance and vacuoles consistent with lipid accumulation (Fig. 7).

Unexpectedly, some animals demonstrated electron-dense immune-type deposits with an organized substructure on examination by electron microscopy (Fig. 6). We therefore decided to examine the deposition of immunoglobulins by immunofluorescence on frozen tissue, in all cases in which frozen tissue had been obtained for special studies, retrospectively. These studies included kidneys from additional mice at ages 72 and 82 weeks that were not part of the original study protocol, but were otherwise without experimental manipulation and hence comparable to study animals except for duration of observation. No significant differences were found between wild-type controls and apoE-/- mice in the semiquantitative scores for the deposition of IgA, IgG, IgM, and C3 at similar ages. Both wild-type mice and apoE-/- mice demonstrated an equivalent increment in glomerular immunoglobulin and C3 deposition with time, resulting in significant differences between age groups.

Table 2. Morphological Data of the Study Groups

	C57BL/6	apoE−/−	apoE−/−
Age (weeks)	36	24	36
n =	6	10	18
Mean macrophages per glomerulus (± SEM)	1.2 (±0.22)	2.5 (±0.34)	4.3 (±0.8)[a]
Percentage of glomeruli with foam cells	0 (±0)	7% (± 1.68)	29% (±4.1)[bc]
Mean glomerular tuft area (μm^2 ± SEM)	3003 (±53)	3399 (±104)	4103 (±130)[bc]
Percentage of glomeruli with lesions of the JG area	0 (±0)	25.5 (±3.7)	59.4 (±3.9)[cd]

JG, juxtaglomerular.
[a] $p < 0.01$ vs C57BL/6.
[b] $p < 0.001$ vs C57BL/6.
[c] $p < 0.05$ vs 24 weeks.
[d] $p < 0.01$ vs 24 weeks.

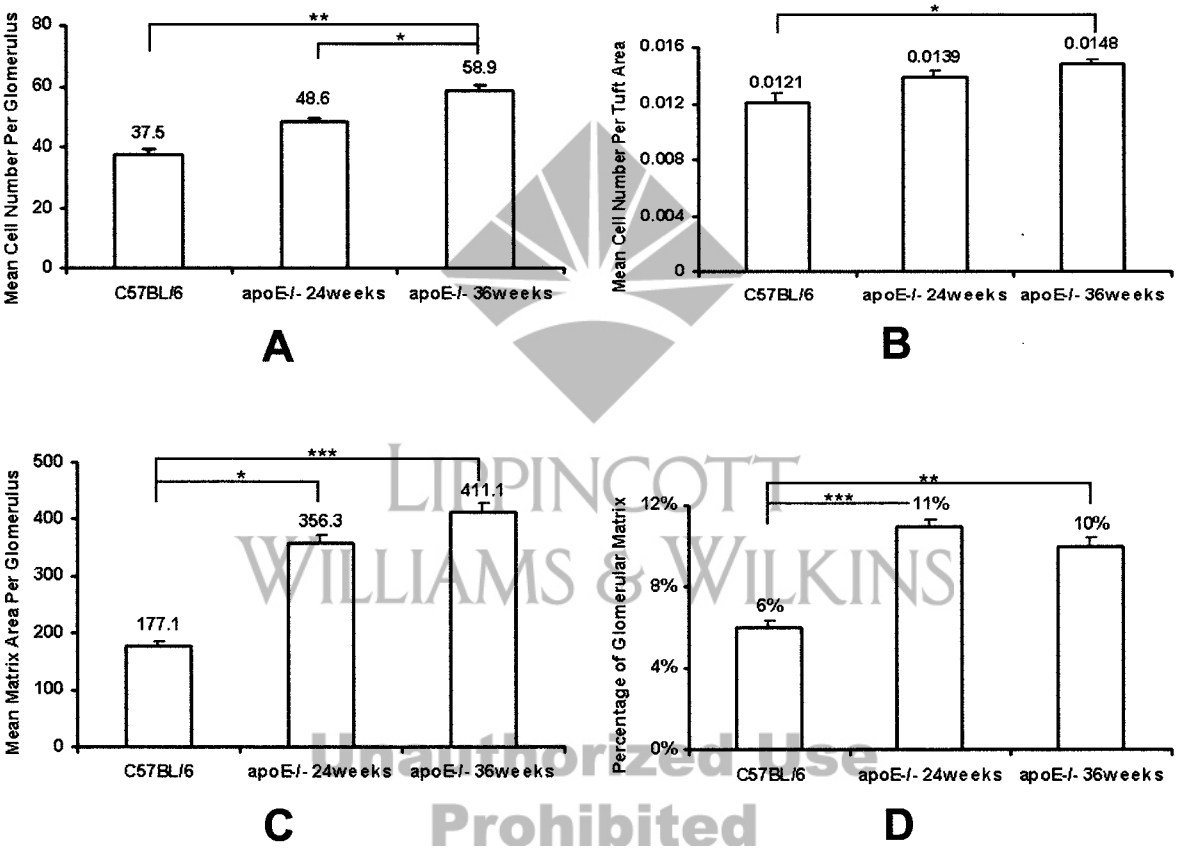

Figure 4.
Mean cell number per glomerulus (A) and per glomerular tuft area (per μm^2) (B). Bars show standard error of the mean (*, $p < 0.05$; **, $p < 0.01$). Mean matrix area per glomerulus (μm^2) (C) and percentage of glomerular matrix (D). Bars show standard error of the mean (*, $p < 0.05$; **, $p < 0.01$, ***; $p < 0.001$).

Discussion

In this study we evaluated a genetically modified mouse strain to define potential effects of hyperlipidemia on renal morphology and ultrastructure. Although apoE-/- mice are widely used as a model system to study atherosclerosis, a detailed description of the renal pathology in this strain has not yet been reported. The pathologic alterations that we document in this strain are the prominent glomerular infiltration with monocytes/macrophages (commonly with foam cell appearance), lipid deposits filling glomerular capillaries, lipid deposits at the vascular pole, and "foamy" degeneration of the arteriolar wall. A distinctive glomerular injury with mesangiolysis, and mesangial expansion resulting from accumulations of lipid-laden monocytes/macrophages and extracellular matrix (specifically including laminin and type IV collagen), and to a much lesser degree, extracellular lipid, also develops in conjunction with these aforementioned changes.

One reason that previous studies may have overlooked renal injury is that many studies of this model have involved much shorter periods of study than that

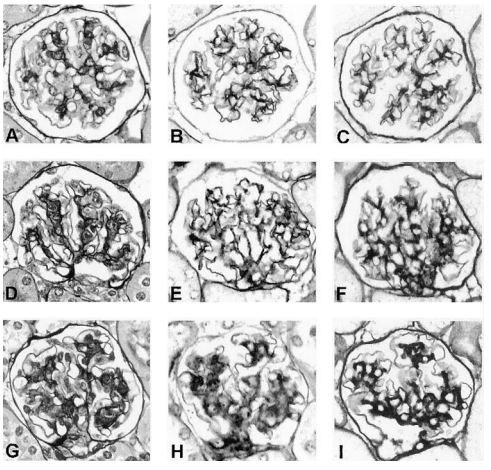

Figure 5.

Characterization of changes in glomerular extracellular matrix in apoE -/- mice. A, B, and C were obtained from wild-type control mice at 24 weeks. D, E, and F are of a representative glomerulus from an apoE-/- mouse at 24 weeks of age, and G, H, and I are of a representative glomerulus from an apoE-/- mouse at 36 weeks of age. A, D, and G are silver methenamine–stained sections. B, E, and H demonstrate immunohistochemical staining for laminin. There is a progressive increase in laminin within the expanded mesangial regions of apoE-/- mice. C, F, and I demonstrate immunohistochemical staining of collagen type IV, which also shows progressive accumulation in the mesangium in conjunction with laminin. Both laminin and collagen IV are increased in apoE-/- mice compared with wild-type control, and this increase in matrix is progressive as the apoE-/- mouse ages from 24 to 36 weeks.

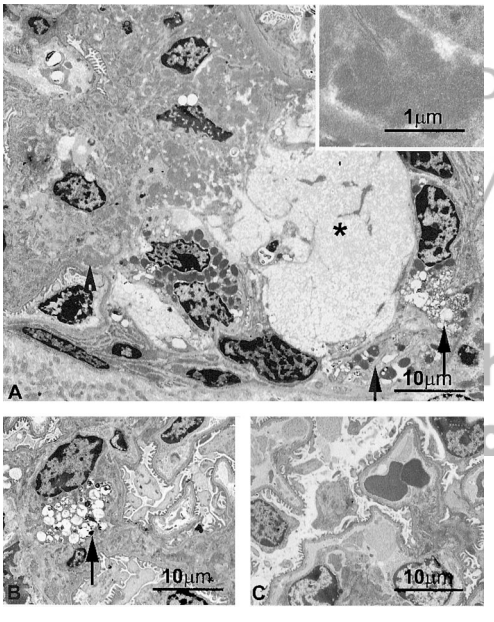

Figure 6.

Ultrastructural changes in apoE-/- mice at 24 weeks of age. Transmission electron microscopy of renal specimens from apoE-/- mice at the age of 24 weeks. A, An overview of a glomerulus with vacuoles consistent with lipid deposits in the juxtaglomerular area (*star*), dense immune deposits in the mesangium (*arrowhead*), and injured arteriolar wall with renin granules and vacuolization of smooth muscle cells (*arrows*). B, A foam cell in the mesangium of a glomerular tuft (*arrows*). C, Normal glomerular tuft from a wild-type control demonstrates the absence of foam cells and lipid deposits.

presented here, and often used animals 10 weeks of age or younger. We demonstrate that age is an important factor in the renal injury identified with clear

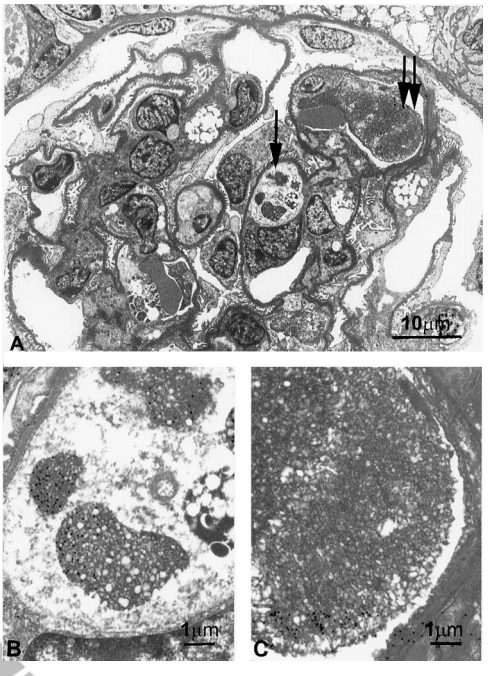

Figure 7.

Ultrastructural features of "lipid thrombi" filling glomerular capillaries. Transmission electron microscopy of renal specimens from apoE-/- mice at the age of 36 weeks. A, Electron microscopic thrombi filling glomerular capillaries were composed of vacuoles consistent with lipid droplets (*arrows*). Area depicted by *single arrow* is illustrated at higher magnification in B, and area depicted by *double arrows* is illustrated in C.

morphologic progression in severity as animals age from 24 to 36 weeks.

The critical role of monocyte/macrophages during glomerular inflammation is well established (Erwig et al, 2001). We found that accumulation of monocyte/macrophages in glomeruli, commonly with foam cell appearance, is a prominent feature in apoE-/- mice with hyperlipidemia. The number of glomerular monocyte/macrophages and the percentage of glomeruli with foam cells rose during the disease time course. As a general comparison, the mean number of glomerular monocyte/macrophages is in the range described for classical immunologic models of glomerular diseases like the nephrotoxic serum nephritis and the apoferritin-induced immune complex glomerulonephritis (Anders et al, 2001; Bird et al, 2000).

One difficulty in determining the exact role of hyperlipidemia in human glomerular diseases is the general presence of multiple factors involved in disease progression. Animal models have allowed the dissection of some of the direct effects of hyperlipidemia on glomerular injury. Several rat strains spontaneously develop hyperlipidemia, including the obese Zucker rat (Zucker, 1965) and the exHC rat (Imai and Matsumura, 1973). Both develop proteinuria and a glomerular lesion characterized by focal glomerular sclerosis and accumulation of lipid-laden foam cells. Therapeutic interventions that reduce lipid levels have been shown to improve kidney function and decrease glomerular injury (Hattori et al, 1994; Kasiske et al, 1988). Additionally, there are a number of reports of

diet induced hyperlipidemia (Kasiske et al, 1990). Rats fed a high cholesterol diet develop glomerular macrophage accumulation, glomerular foam cells, and mild proteinuria during a 6-week time course. These lesions are consistent with the findings in apoE-/- mice (Hattori et al, 1999).

Activation of intrinsic glomerular cells leading to the induction of adhesion molecules and release of chemoattractants is thought to be responsible for the glomerular macrophage accumulation in various animal models of glomerular injury. Support for this idea is provided both by in vitro and in vivo data. In the above-mentioned rat model, an induction of macrophage colony stimulating factor (M-CSF) has been demonstrated as one potential macrophage chemoattractant (Hattori et al, 1999). In vitro studies demonstrated the induction of M-CSF and the chemokine CCL2 (MCP-1) by mesangial cells exposed to LDL or oxidized LDL (Kamanna et al, 1996; Kim et al, 1995). Therefore, increased LDL in the circulation and oxidation after glomerular deposition might activate mesangial cells to release chemoattractants, which elicits glomerular inflammation, a process similar to experimental models of immune glomerular injury (Segerer et al, 2000).

About 50% of apoE-/- mice at the age of 36 weeks demonstrated glomerular capillaries filled with somewhat amorphous, but discrete accumulations of acellular material, resembling lipid deposits. This lesion seems to develop late in the disease course, because none of the animals at 24 weeks of age had evidence of this lesion. A human disease with similar findings of "lipoprotein thrombi" filling glomerular capillaries is lipoprotein glomerulopathy (LPG) (Saito et al, 1999). LPG is a rare renal disorder, found mainly in Japanese patients, and is associated with mutant apoE alleles, like apoE Sendai. A recent study used a virus-mediated transduction of apoE Sendai into apoE-deficient mice (Ishigaki et al, 2000). The authors described "lipoprotein thrombi" in expanded glomerular capillaries resembling LPG, which developed only in apoE-deficient mice transfected with apoE Sendai, but not in controls, and concluded that apoE Sendai is an etiologic cause of LPG (Ishigaki et al, 2000). Our study indicates that apoE deficiency in the genetic background of murine C57BL/6, leading to hyperlipidemia, is sufficient for the development of these features, which resemble human LPG, and that the Sendai mutation of apoE is not a requirement for this injury to develop.

The juxtaglomerular apparatus consisting of the macula densa, the extraglomerular mesangium, and afferent and efferent arteriole is of major importance in the regulation of the renal microvasculature, hemodynamics, and blood pressure (Persson and Bachmann, 2000). In apoE-/- mice, lipid deposits and foam cells are present at this important anatomical site. Some but not all lipid deposits were present in the wall of arterioles, most likely resulting in foam cells derived from smooth muscle cells. Therefore, in apoE-deficient mice, renal foam cells seem to derive from different cell sources, namely, vascular smooth muscle cells in the vascular pole and monocyte/macrophages in the glomerular tuft. Because different LDL modifications lead to foam cell formation in different cell types, it will be interesting to further define the composition of lipid deposits at different sites in the kidney (Llorente-Cortes et al, 2000; Tertov et al, 1992). These studies have not been performed herein, because we were mainly limited to fixed material in this animal series. It is likely that the morphologic changes with lipid deposits in the juxtaglomerular apparatus and foam cell formation in arterioles impairs microvascular regulation in apoE-/- mice. The role of these findings during the potential development of hypertension in these mice is currently unknown (Yang et al, 1999).

An unexpected finding in some animals was the demonstration of electron-dense immune-type deposits with an organized substructure on examination by electron microscopy. No significant differences were found between wild-type controls and apoE-/- mice for the deposition of immunoglobulins or complement at similar ages. However, both wild-type mice and apoE-/- mice demonstrated an equivalent increment in glomerular immunoglobulin and C3 deposition with time, resulting in significant differences between age groups. These observations indicate that the glomerular immunoglobulin deposition in the mice was not related to hyperlipidemia or apoE deficiency, but reflected a nonspecific process associated with aging, in agreement with what is known to occur normally in many strains of mice.

In summary, apoE-deficient mice with severe hyperlipidemia developed progressive glomerular lesions. The main morphologic alterations consisted of glomerular macrophage infiltration with foam cell formation, lipid deposits filling glomerular capillaries, lipid deposits in the juxtaglomerular area with foam cell appearance of arteriolar smooth muscle cells and, at times, mesangiolysis. Gene-targeted mouse strains on defined genetic backgrounds have proven to be powerful tools to dissect the complex interactions during renal injury. ApoE-deficient mice offer an important opportunity to study the effects of hyperlipidemia and combinations of hyperlipidemia and other risk factors on renal disease. Degeneration of smooth muscle cells of the arteriolar wall into foam cells and glomerular macrophage infiltration might set the stage in which additional stresses drive progression of both glomerular and vascular injury. Although blood pressure was not specifically measured in this study, this study suggests that use of this murine model for studies of cardiovascular disease that involve a component of hypertension will need to consider potential contributions of renal injury to pathophysiologic alterations.

Material and Methods

Animals

Female apoE-/- and wild-type C57BL/6 mice, age 8 to 10 weeks, were purchased from the Jackson Laboratory (Bar Harbor, Maine). Mice were fed a pelleted rodent chow (Harlan Teklad, Madison, Wisconsin)

containing 4% fat, 24% protein, 4.5% crude fiber, and 0.01% BHT (manufacturer's estimates) until the ages of 24 and 36 weeks. Mice were maintained in a temperature-controlled room (22° C) with a 12-hour light/dark cycle and were given free access to food and water. Food was removed from the mice 4 hours before the collection of blood from the retro-orbital plexus. Serum was stored at −70° C until analysis. Mice were killed under ether narcosis by cervical dislocation and whole animals were perfused with 10 ml of antioxidant buffer (100 μM DTPA, 100 μM BHT, 0.1% ethanol, in PBS, pH 7.4) via the left ventricle. Additionally, frozen kidney tissue suitable for immunofluorescence staining was available from apoE-/- mice at 24 ($n = 10$) and 82 weeks ($n = 4$) of age and from C57Bl/6 mice at 36 ($n = 6$) and 72 weeks ($n = 4$). The mice at the very late time points (72 and 82 weeks) were not originally included in the study, but these tissues for immunofluorescence studies were used to evaluate an unexpected morphologic finding of possible immune complex deposition revealed by electron microscopic studies, as detailed below. This electron microscopic finding was obtained after all animals enrolled in the studies had been killed and suitable tissue for immunofluorescence was no longer available. All animal studies were reviewed and approved by the Animal Care Committee of the University of Washington.

Plasma Lipids

Plasma cholesterol levels were determined using a colorimetric kit (Diagnostic Chemicals Limited, Oxford, Connecticut) with cholesterol standards (Preciset #12552; Boehringer Mannheim, Indianapolis, Indiana). Plasma triglyceride levels were determined colorimetrically after removal of free glycerol (Diagnostic Kit #450032; Boehringer Mannheim).

Tissue Preparation and Microscopic Examination

Kidneys were removed and in part fixed in 10% neutral buffered formalin, in methyl Carnoy's solution (60% methanol, 30% chloroform, 10% acetic acid), and in half-strength Karnovsky's solution (1% paraformaldehyde and 1.25% glutaraldehyde in 0.1 M sodium cacodylate buffer, pH 7.0). Formalin and methyl Carnoy's fixed kidneys were processed and embedded in paraffin following standard protocols. Sections 2-μm thick were stained with hematoxylin-eosin (HE) and periodic acid-methenamine silver (PAM). Selected cases were snap-frozen in liquid nitrogen and stored at −70° C.

Electron Microscopy

The protocols used for electron microscopy have previously been described in detail (Alpers et al, 1993; Namimatsu, 1992).

Immunohistochemistry

The protocols for immunohistochemistry have previously been described in detail (Anders et al, 2001; Segerer et al, 2000). Primary antibodies used were a monoclonal anti–smooth muscle actin (SMA) antibody (IgG2A, clone 1A4; Dako, Carpinteria, California), a rat anti-mouse MAC-2 antibody (clone M3/38; Cedarlane, Ontario, Canada), an antibody against PCNA (IgG2A, clone PC10; Calbiochem, San Diego, California), a goat anti–type IV collagen (Southern Biotechnology Associates, Birmingham, Alabama), and rabbit anti-laminin antibody (Chemicon International, Temecula, California). All antibodies have been used in previous studies for immunohistochemistry on paraffin embedded tissue (Alpers et al, 1993; Bird et al, 2000; Nangaku et al, 2002; Shankland et al, 2000). Secondary antibodies were a biotinylated anti-rat IgG (Vector, Burlingame, California), and an anti-mouse IgG2A antibody (PharMingen, San Diego, California). 3,3'-diaminobenzidine with nickel enhancement, resulting in a black product, was used as chromogen.

Immunofluorescence

Sections 8-μm thick were used for immunofluorescence. The sections were fixed in acetone, air-dried, and rehydrated in PBS. Incubation with normal goat serum was followed by incubation with fluorescein-5-isothiocyanate (FITC)–conjugated goat anti-mouse IgA, IgG, IgM, and C3 (all from Cappel Pharmaceuticals, Aurora, Ohio) for 30 minutes. Sections were washed in PBS and cover slipped in aqueous mounting media.

Quantitative Analysis and Statistics

HE- and PAM-stained tissue sections were used for morphometric analysis. Fifteen consecutive glomerular cross-sections were photographed by an examiner, blinded to the source of the tissue, using a digital camera (Olympus DP11; Olympus America, Melville, New York), and imported into Image-Pro Plus (Media Cybernetics, Silver Spring, Maryland). Number of nuclei, area of mesangial matrix, and glomerular tuft area were quantified for each glomerular cross-section. The number of MAC-2–positive monocyte/macrophages and PCNA-positive cells were counted in 30 glomeruli per slide. Each glomerulus with the vascular pole present in the cross-section was evaluated on every slide for the presence of foam cells within the glomerulus, and the presence of foam cells in the walls of the afferent and efferent arterioles. The immunofluorescence staining was quantified in 15 glomeruli per slide. Fluorescence intensity was graded semiquantitatively on a scale from 0 (negative) to 4 (very strong).

Using the InStat program (Version 3.0 for Windows; Intuitive Software for Science, San Diego, California), the mean numbers were compared using the nonparametric Kruskal-Wallis test and the Dunn's multiple comparison. A $p < 0.05$ was considered to be statistically significant.

References

Alpers CE, Seifert RA, Hudkins KL, Johnson RJ, and Bowen-Pope DF (1993). PDGF-receptor localizes to mesangial, pa-

rietal epithelial, and interstitial cells in human and primate kidneys. Kidney Int 43:286–294.

Anders HJ, Vielhauer V, Kretzler M, Cohen CD, Segerer S, Luckow B, Weller L, Grone HJ, and Schlondorff D (2001). Chemokine and chemokine receptor expression during initiation and resolution of immune complex glomerulonephritis. J Am Soc Nephrol 12:919–931.

Attman PO, Alaupovic P, and Samuelsson O (1999). Lipoprotein abnormalities as a risk factor for progressive nondiabetic renal disease. Kidney Int Suppl 71:S14–17.

Bird JE, Giancarli MR, Kurihara T, Kowala MC, Valentine MT, Gitlitz PH, Pandya DG, French MH, and Durham SK (2000). Increased severity of glomerulonephritis in C-C chemokine receptor 2 knockout mice. Kidney Int 57:129–136.

Erwig LP, Kluth DC, and Rees AJ (2001). Macrophages in renal inflammation. Curr Opin Nephrol Hypertens 10:341–347.

Fazio S and Linton MF (2001). Mouse models of hyperlipidemia and atherosclerosis. Front Biosci 6:D515–525.

Ghiselli G, Schaefer EJ, Gascon P, and Breser HB Jr (1981). Type III hyperlipoproteinemia associated with apolipoprotein E deficiency. Science 214:1239–1241.

Hattori M, Ito K, Kawaguchi H, and Yamaguchi Y (1994). Probucol reduces renal injury in the ExHC rat. Nephron 67:459–468.

Hattori M, Nikolic-Paterson DJ, Miyazaki K, Isbel NM, Lan HY, Atkins RC, Kawaguchi H, and Ito K (1999). Mechanisms of glomerular macrophage infiltration in lipid-induced renal injury. Kidney Int Suppl 71:S47–50.

Imai Y and Matsumura H (1973). Genetic studies on induced and spontaneous hypercholesterolemia in rats. Atherosclerosis 18:59–64.

Ishigaki Y, Oikawa S, Suzuki T, Usui S, Magoori K, Kim DH, Suzuki H, Sasaki J, Sasano H, Okazaki M, Toyota T, Saito T, and Yamamoto TT (2000). Virus-mediated transduction of apolipoprotein E (ApoE)-sendai develops lipoprotein glomerulopathy in ApoE-deficient mice. J Biol Chem 275: 31269–31273.

Kamanna VS, Pai R, Roh DD, and Kirschenbaum MA (1996). Oxidative modification of low-density lipoprotein enhances the murine mesangial cell cytokines associated with monocyte migration, differentiation, and proliferation. Lab Invest 74:1067–1079.

Kasiske BL, O'Donnell MP, Cleary MP, and Keane WF (1988). Treatment of hyperlipidemia reduces glomerular injury in obese Zucker rats. Kidney Int 33:667–672.

Kasiske BL, O'Donnell MP, Schmitz PG, Kim Y, and Keane WF (1990). Renal injury of diet-induced hypercholesterolemia in rats. Kidney Int 37:880–891.

Keane WF (2000). The role of lipids in renal disease: Future challenges. Kidney Int Suppl 75:S27–31.

Kim SY, Guijarro C, O'Donnell MP, Kasiske BL, Kim Y, and Keane WF (1995). Human mesangial cell production of monocyte chemoattractant protein-1: Modulation by lovastatin. Kidney Int 48:363–371.

Knowles JW, Reddick RL, Jennette JC, Shesely EG, Smithies O, and Maeda N (2000). Enhanced atherosclerosis and kidney dysfunction in eNOS(-/-)Apoe(-/-) mice are ameliorated by enalapril treatment. J Clin Invest 105:451–458.

Llorente-Cortes V, Martinez-Gonzalez J, and Badimon L (2000). LDL receptor-related protein mediates uptake of aggregated LDL in human vascular smooth muscle cells. Arterioscler Thromb Vasc Biol 20:1572–1579.

Mahley RW and Huang Y (1999). Apolipoprotein E: From atherosclerosis to Alzheimer's disease and beyond. Curr Opin Lipidol 10:207–217.

Majumdar A and Wheeler DC (2000). Lipid abnormalities in renal disease. J R Soc Med 93:178–182.

Nakashima Y, Plump AS, Raines EW, Breslow JL, and Ross R (1994). ApoE-deficient mice develop lesions of all phases of atherosclerosis throughout the arterial tree. Arterioscler Thromb 14:133–140.

Namimatsu S (1992). Periodic acid thiosemicarbazide gelatin methenamine silver (PATSC-GMS) staining for transmission electron microscopy. J Submicrosc Cytol Pathol 24:19–28.

Nangaku M, Pippin J, and Couser WG (2002). C6 mediates chronic progression of tubulointerstitial damage in rats with remnant kidneys. J Am Soc Nephrol 13:928–936.

Persson AE and Bachmann S (2000). Constitutive nitric oxide synthesis in the kidney: Functions at the juxtaglomerular apparatus. Acta Physiol Scand 169:317–324.

Plump AS, Smith JD, Hayek T, Aalto-Setala K, Walsh A, Verstuyft JG, Rubin EM, and Breslow JL (1992). Severe hypercholesterolemia and atherosclerosis in apolipoprotein E-deficient mice created by homologous recombination in ES cells. Cell 71:343–353.

Reddick RL, Zhang SH, and Maeda N (1994). Atherosclerosis in mice lacking apo E: Evaluation of lesional development and progression. Arterioscler Thromb 14:141–147.

Saito T, Oikawa S, Sato H, and Sasaki J (1999). Lipoprotein glomerulopathy: Renal lipidosis induced by novel apolipoprotein E variants. Nephron 83:193–201.

Segerer S, Cui Y, Hudkins KL, Goodpaster T, Eitner F, Mack M, Schlondorff D, and Alpers CE (2000). Expression of the chemokine monocyte chemoattractant protein-1 and its receptor chemokine receptor 2 in human crescentic glomerulonephritis. J Am Soc Nephrol 11:2231–2242.

Shankland SJ, Eitner F, Hudkins KL, Goodpaster T, D'Agati V, and Alpers CE (2000) Differential expression of cyclin-dependent kinase inhibitors in human glomerular disease: Role in podocyte proliferation and maturation. Kidney Int 58:674-683.

Stevenson FT and Kaysen GA (1999). Hyperlipidemia and renal disease: The use of animal models in understanding pathophysiology and approaches to treatment. Wien Klin Wochenschr 111:307–314.

Tertov VV, Orekhov AN, Sobenin IA, Gabbasov ZA, Popov EG, Yaroslavov AA, and Smirnov VN (1992). Three types of naturally occurring modified lipoproteins induce intracellular lipid accumulation due to lipoprotein aggregation. Circ Res 71:218–228.

Yang R, Powell-Braxton L, Ogaoawara AK, Dybdal N, Bunting S, Ohneda O, and Jin H (1999). Hypertension and endothelial dysfunction in apolipoprotein E knockout mice. Arterioscler Thromb Vasc Biol 19:2762–2768.

Zucker LM (1965). Hereditary obesity in the rat associated with hyperlipemia. Ann NY Acad Sci 131:447–458.